PFC/JA-90-35

Operation of a Long-Pulse CARM Oscillator

Pendergast, K.D.; Danly, B.G.; Temkin, R.J.

Plasma Fusion Center
Massachusetts Institute of Technology
Cambridge, MA 02139

September 1990

Submitted to: Nuclear Instruments & Methods (special issue).

This work was supported by U.S. D.O.E. Contract DE-FG02-89ER-14052.

ABSTRACT

A long-pulse (1 μsec), millimeter-wave cyclotron autoresonance maser (CARM) oscillator experiment has been carried out. A SLAC 5045 klystron gun produced an electron beam at 250-320 kV and 10-20 A; a beam $\alpha \equiv p_\perp/p_\parallel$, variable from 0 to 1, was produced on this electron beam with a wiggler magnetic field near guide field resonance. The experiments were carried out with two different Bragg reflection resonators designed for the TE_{11} mode. Using the first resonator, many harmonic gyrotron modes were observed in the 28.2-40.1 GHz frequency range in the TE_{21}, TE_{01}, TE_{31} modes near cutoff and, for the first time, a second harmonic upshifted (CARM) TE_{11} mode at 74.5 GHz was observed. Using the second resonator, fundamental CARM operation was observed for many parameter settings, and for frequencies ranging from 29 to 32 GHz. Identification of these CARM modes is made by comparison of measured frequencies with uncoupled dispersion theory and measurement of the farfield radiation pattern. Output powers ranged from $\sim$ 0.1 kW to 100 kW, resulting in efficiencies of 0.1% to 3%.

I. Introduction

A promising candidate for the efficient generation of coherent electromagnetic radiation in the millimeter and sub-millimeter regimes is the cyclotron autoresonance maser (CARM). Operation of a short-pulse CARM oscillator experiment in the Soviet Union has been reported,[1] and the design of a CARM oscillator at 100 GHz has also been performed at NRL.[2] There has been much work on the theory and design of CARMs[3-8] and a success in the operation of a short-pulse CARM amplifier at 35 GHz.[9]

So far, operation of a long-pulse CARM oscillator has not been achieved.For multiple-pass oscillator designs, the time required for the rf power to reach equilibrium may be several tens of nanoseconds for high-Q cavities, so long-pulse ($\geq 1\mu$sec) operation is desirable for efficient operation. Long-pulse operation of CARMs may be promising for applications as an ECRH source for fusion plasmas and utilizes conventional modulator technology to achieve high-average power rf output. For applications using CARMs as drivers for rf linacs, pulse compression techniques may be used to achieve high peak power rf output.

The frequency output from a CARM is determined by the resonance condition

$$\omega = n\Omega_c + k_{||}v_{||}, \tag{1}$$

where in a cavity ω must satisfy a cavity-mode solution to Maxwell's equations. In Eq. 1, $\Omega_c = \Omega_{c0}/\gamma = eB_0/m\gamma$ is the relativistic cyclotron frequency, $\gamma = E/mc^2$ is the relativistic energy factor, B_0 is the uniform axial magnetic field, $k_{||}$ is the axial wavenumber, n is the harmonic number, and $v_{||}$ is the axial component of the electron beam velocity. Eq. 1 may be rewritten as

$$\omega = \frac{n\Omega_c}{\left(1 - \beta_{||}/\beta_{ph}\right)}, \tag{2}$$

where $\beta_{||} = v_{||}/c$, and $\beta_{ph} = \omega/ck_{||}$ is the normalized wave phase velocity. A principle advantage of the CARM over the gyrotron ($\beta_{ph} \rightarrow \infty$) is the large Doppler upshift of the operating frequency from the cyclotron frequency, Ω_c, resulting from wave phase velocities where $\beta_{ph} \sim 1$.

Because of the Doppler-shift term in the resonance condition it may be concluded that a large spread in the axial velocity distribution will greatly decrease the number of resonant electrons, and CARM performance will be seriously diminished. A simple coherence argument yields an estimate of the maximum allowable axial velocity spread in the electron beam. If two electron have phases that differ by more than π at the end of the interaction, then they cannot coherently interact with the rf. Using this condition with paritcle axial velocities $v_{\|_1}$ and $v_{\|_2}$ such that $v_{\|_1} + v_{\|_2} = 2v_{\|}$ and $v_{\|_1} - v_{\|_2} = \Delta v_{\|}$, then in the small signal limit:

$$\frac{\Delta v_{\|}}{v_{\|}} \leq \frac{\lambda}{2L} \left\{ \frac{(1-\gamma^{-2})^{1/2}}{(1+\alpha^2)^{1/2}\left(1-\frac{\Omega_c}{\omega}\right)} \right\}. \tag{3}$$

where $\alpha = v_\perp / v_{\|}$ is the pitch angle and L is the interaction length. If L = 0.2 m, ν = 37.5 GHz, $\gamma = 1.881$, $\alpha = 0.6$, and $B_0 = 8.45$ T, then Eq. 3 gives a maximum allowable axial velocity spread of 2.2%.

In general, there are two intersections on an $\omega - k$ dispersion diagram between the beamline which satisfies the resonance condition (Eq. 1) and an uncoupled waveguide mode; the frequencies of the two intersections are given by

$$\omega = \frac{n\gamma_{\|}^2}{\gamma}\Omega_{c0} \left\{ 1 \pm \sqrt{1 - \frac{1}{\gamma_{\|}^2}\left(1 + \left(\frac{\gamma\beta_{\|}\omega_c}{n\Omega_{c0}}\right)^2\right)} \right\}. \tag{4}$$

The CARM interaction frequency is the upshifted intersection (+), where small changes in α can lead to large variations in frequency. The downshifted intersection (−) generally corresponds to beam interaction with a wave at much larger phase velocity (gyrotron interaction).

II. Experimental Design

Here we present the design of a long-pulse, 450 kV, 37.5 GHz CARM oscillator experiment at MIT. A schematic of the experiment is shown in Fig. 1. A high-voltage 2.5 μsec (1 μsec flattop) pulse-modulator[10] provides the accelerating potential to a Pierce-type electron gun which emits a solid axi-centered electron beam into a uniform magnetic field. The emitted electron beam has very little perpendicular momentum as it enters a bifilar helical

(Pierce) wiggler and resonantly interacts with a rotating transverse magnetic field which converts parallel momentum to perpendicular momentum. Upon exit of the wiggler region, the electron beam is adiabatically compressed into the high-field region where the CARM interaction takes place. The two uniform magnetic field regions, that in the wiggler region and in the interaction region, are provided by a superconducting magnet which allows the fields to be varied independently. In this paper, we will briefly describe the design of the components of the CARM oscillator experiment. In addition, the results of the experiment will be presented, and a comparison with theory will be made.

The design of the magnetic focusing system to compress the electron beam from the cathode into the uniform field of the wiggler was carried out with the objective to optimize the beam quality within engineering constraints. To achieve this, the ray-tracing code EGUN[11] was used to simulate the electron trajectories and POISSON/MIRT code group[12] was used to calculate and optimize a set of coils and iron pole pieces to fit a desired magnetic field profile.

A bifilar helical wiggler is used to convert parallel beam energy to perpendicular beam energy before the electrons enter the CARM interaction region. The design of the bifilar helical wiggler was performed with the use of the particle trajectory code TRAJ, which was developed at MIT. In TRAJ, particles are loaded with some initial spread in energy and parallel momentum, and then the equations of motion are integrated along the axis of the wiggler. The fields include a rotating perpendicular magnetic field produced by the wiggler, an externally-applied uniform guide magnetic field, and the space-charge electric field and self-B_θ fields that are generated by the beam. The helical windings of the coil are approximated by ideal current elements and the magnetic field is then calculated at the position of the particle. At the output of the wiggler, the final values of average energy, $< \gamma >$, average pitch angle, $< \alpha >$, and velocity spread of the electron beam are calculated. Shown in Fig. 2 is a typical case where the average pitch angle, is plotted as a function of the axial distance from the start of the wiggler to the start of the interaction region. By continuously varying the wiggler current, the pitch angle at the end of the wiggler region may also be continuously varied. To calculate the values of beam pitch angle in the CARM oscillator experiment, the particles are loaded in TRAJ according to the position and phase space of the output rays of EGUN so that realistic values for the velocity and energy spread

may be obtained. The wiggler guide field was set near the resonance field[13] $B_{\rm res} = \frac{mc^2}{e}\beta\gamma k_w$, which varies with voltage.

The resonator used in the CARM oscillator experiment is of the Bragg- reflection type. This resonator consists of a straight cylindrical waveguide section with rippled wall reflectors at both ends; such a resonator allows passage of the electron beam while at the same time exhibiting a high diffractive Q, Q_D, for resonant modes. The Bragg reflectors have a periodic wall structure with radius $R(z) = R_w + \delta R\cos(2\pi z/\lambda_b + \phi_b)$, where λ_b and ϕ_b are the periodicity and phase of the wall perturbations, respectively. These reflectors are designed to achieve a desired reflectivity and mode selectivity for modes which satisfy the Bragg resonance condition:

$$\lambda_g = 2\lambda_b, \tag{5}$$

where $\lambda_g = 2\pi/k_{||}$ is the guide wavelength. A schematic of the two Bragg resonators used in this experiment is shown in Fig. 3. Theoretical calculations for reflectivity and mode selectivity of Bragg resonators and mode coupling in corrugated structures has been presented in earlier studies .[14-16] For the CARM oscillator experiment, the Bragg resonator was designed to operate at 37.5 GHz. The upstream reflector has more ripple periods than the downstream reflector for higher reflectivity. For a given frequency, mode, length of the cavity, and power reflectivities of the upstream (R_u) and downstream (R_d) reflectors, the diffractive Q of the cavity, Q_D, can be approximated by

$$Q_D \approx \frac{k^2 L}{k_{||}\left(1-(R_u R_d)^{\frac{1}{2}}\right)}. \tag{6}$$

The design parameters for the Bragg cavity are shown in Table 1. For the first Bragg resonator studied, the waveguide radius of the straight section in the resonator was equal to the radius corresponding to the ripple maxima of the reflectors. This configuration from here on will be referred to as Cavity #1. A second set of experiments were carried out with a resonator in which a new straight section was inserted; this straight section had a radius corresponding to the ripple minima of the reflectors and will be referred to as Cavity #2. Because the same reflectors were used for both of the cavities, Cavity #2 has a step of magnitude 2 δR = 0.5 mm in the reflector/straight section interfaces.

III. Experimental Results

In this section, we present results from the long-pulse CARM oscillator experiment at MIT. The CARM oscillator experiment operated in pulsed mode where the time between pulses was limited by vacuum pressure. Typical pulse repetition rates were 1/3 Hz; a maximum repetition rate of 1 Hz was achieved for 10-20 pulses for performing calorimetric measurements. The voltage on the electron gun was limited to $\sim$ 320 kV (instead of the 450 kV design voltage), also because of the vacuum pressure. One of the contributing factors to the relatively high background pressure in the vacuum was due to the utilization of an emittance selector in the focusing region to limit the size of the electron beam entering the resonator.

Separate Rogowski current transformers on the beam tunnel, resonator, and collector were used to measure the beam current that penetrated the emittance selector. All of the quoted beam currents are those measured from the collector pipe only. There was negligible current measured from the resonator, but nonzero currents were measured on the beam tunnel in cases where the wiggler current was relatively high (corresponding to large beam α). In all cases where an rf signal was observed, the magnetic coils in the electron beam focusing system were varied to optimize the magnitude of the signal and the collector current.

The operating parameters for the CARM oscillator experiment are shown in Table 2. The voltage, wiggler current, and the axial magnetic field strengths of the wiggler region and the interaction region were variable, and the frequency of the resulting rf emission was measured with a SAW spectrometer. Farfield scans were performed for modes where the rf signal did not vary pulse-to-pulse. Power measurements were performed using both a calibrated diode and calorimetry.

In the case of the first cavity (Cavity #1), multimode emission was observed, and many of the modes were identified in the frequency range 28.2-40.1 GHz. These modes correspond to second (n=2) and third (n=3) harmonic TE modes (TE_{21}, TE_{01}, and TE_{31}) using a simple dispersion analysis with uncoupled waveguide modes. These modes all corresponded to the down-shifted frequency intersection where $\omega \approx n\Omega_c$ with n=2,3. Also observed was a low-power mode at 74.5 GHz corresponding to the upshifted (CARM) TE_{11} mode at second harmonic (n=2).

Because of the predominance of oscillation on modes near cutoff in Cavity #1, Cavity #2 was fabricated to reduce the anomalously high Q for modes near cutoff. The straight section radius of Cavity #2 was decreased to match the miminum radius of the rippled sections. The observed modes for this cavity are shown in Table 3. In this case, there was single-mode emission in the TE_{11} mode in the frequency range 29-32 GHz for many parameter settings. Using measured values of voltage, wiggler current, and magnetic field, the γ, $\gamma_{\|}$, Ω_{c0}, and $\beta_{\|}$ in Eq. 4 may be found, leaving the mode and harmonic number (n) as unknowns. The values of α were obtained by simulation from EGUN and TRAJ with realistic beam quality values. Identification of a mode at a particular harmonic is achieved when the measured frequency agrees with the frequency calculated from Eq. 4. Measured frequencies for most of the rf signals using Cavity #2 agreed with the frequencies calculated using this uncoupled dispersion analysis. The dispersion diagram for one observed mode in Ka-band is shown in Fig. 4. In addition, far-field patterns were obtained and compared with theory; a typical case is shown in Fig. 5.

The frequency measurements were performed using a heterodyne receiver and a surface acoustic wave (SAW) dispersive delay-line filter. The mixer combined the CARM signal (ν_{RF}) with a local oscillator (ν_{LO}) obtained from a YIG-tuned Gunn oscillator. The local oscillator was tuned to yield a 1 GHz intermediate frequency (ν_{IF}), with $\nu_{RF} = \nu_{LO} \pm \nu_{IF}$. The single-shot bandwidth and resolution of the SAW spectrometer are 400 MHz and 8 MHz, respectively. In most of the observed modes, the frequency spectrum showed narrow-band (10 MHz) emission. In some cases, multiple-mode spectra was observed.

Power estimates of the rf signal were performed with both a calibrated diode measurement in the farfield of the radiation pattern and a calorimetric measurement; there was rough agreement (factor of $\sim 2\times$) between the two methods. Powers in the TE_{11} modes were observed up to ≈ 3 kW at V ≤ 300 kV.

Also observed were two modes at a voltage of 317 kV and a current of 10 A, where powers near 100 kW were observed with a diode calibration measurement assuming a TE_{11} upshifted mode at 30 GHz. Strong rf breakdown occured at the output window for operation at these parameters.

Preliminary results from cold-tests of Cavity #2 showed resonances near the design frequency (37.5 GHz) and also in the 29-32 GHz frequency band. Measured power reflectivities

of the Bragg reflectors were lower than the values calculated analytically from coupled mode theory. For the large reflector, the measured reflectivity was $R_u \sim 65$ % and for the small reflector the measured reflectivity was $R_d \sim 17$ %.

IV. Discussion

There is strong evidence that the observed modes were upshifted (CARM) modes. For most of the modes observed in Cavity #2, the pitch angle values given by the EGUN and TRAJ codes yield intersections with the uncoupled waveguide modes at frequencies very close to the measured frequency, as was seen in Fig. 4. A notable exception is for modes 43 and 44, where there is not good agreement with the uncoupled dispersion theory. Measured farfield radiation patterns agree very well with theoretical estimates for the TE_{11} design mode. The cavity cold-tests indicated that $k_{||} \gg k_{\perp}$ for the resonant modes, so these modes must be far from cutoff.

Cold-beam theoretical estimates using a constant-field profile in a nonlinear single particle calculation (for example Fliflet[2]) of the efficiency of the CARM oscillator at operating voltages ($\sim$ 300 kV) using measured values of Q ($\sim$ 220) and frequency ($\sim$ 30 GHz) are $\sim$ 2.5 %. This contrasts with $\sim$ 18 %, calculated using the design voltage (450 kV) and frequency (37.5 GHz). Axial velocity spread will decrease the efficiency and account for the low output powers observed. The modes shown in Table 3 have axial velocity spreads calculated from the computer code TRAJ to be in the range of 1-5%, and the maximum allowable axial velocity spreads were calculated from Eq. 3 to be in the range of 2-3 %. EGUN simulations indicate that the electron beam transport yields considerably lower beam quality at lower voltages than the design voltage. It appeared near the end of the operation of the CARM oscillator experiment that higher beam voltages yielded considerably larger output powers in the rf signals, indicating that the beam quality was improving.

Both the design frequency (37.5 GHz) and lower frequencies (29-32 GHz) were observed in the cavity cold test, but the CARM oscillator operated primarily in the 29-32 GHz range for Cavity #2. Since the measured reflectivities of the Bragg reflectors were lower than the design values, the resonant Q of the resonator will be reduced. In addition, the operating voltage ($\leq$320 kV) was considerably lower than the design voltage (450 kV). This required

a reduction of beam α for resonance with the design 37.5 GHz TE_{11} mode of the Bragg resonator, and a corresponding increase in the starting current. The starting current will also increase as the velocity spread in the beam increases. Then as $I_b \rightarrow I_{start}$, the start-oscillation time will increase. So the combination of low Q's and high starting currents might explain why there was not operation of the CARM oscillator at 37.5 GHz. The coupling mechanism of the modes in the 29-32 GHz band is not well understood. One possible explanation is mode conversion from TE_{11} to TM_{11} in the reflectors, and reflection of the TM_{11} mode which is near cutoff at these frequencies.

V. Summary

In summary, we have carried out the first successful long-pulse CARM oscillator experiment. Operation using Cavity #1 showed dominant operation in TE_{21}, TE_{01}, and TE_{31} modes near cutoff at the second and third harmonic in the frequency range 28.2-40.1 GHz. Also, a second harmonic CARM mode at 74.5 GHz at low power was observed. Operation using Cavity #2 showed operation in TE_{11} mode at the CARM intersection at 29-32 GHz. Powers of up to 3 kW were observed for the identified modes. Two high-power ($\sim$ 100 kW) modes were observed in the Ka band for V=317 kV, I=10 A, but the frequency was not measured. The frequency spectrum showed narrow band emission for most of the observed modes and some multiple mode spectra were observed. Preliminary cold-tests of Cavity #2 showed resonances near the design frequency (37.5 GHz) and in the 29-32 GHz band. Although efficiencies in the identified modes were relatively low ($\sim$ 0.1 %), they can be attributed to poor beam quality and lower operating voltages than that for which the CARM oscillator was originally designed.

VI. Acknowledgements

This work was supported by the U.S. Department of Energy, Office of Basic Energy Sciences, Contract DE-FG02-89ER 14052. We thank the klystron division of Stanford Linear Accelerator Center for providing the 5045 klystron gun used in these experiments.

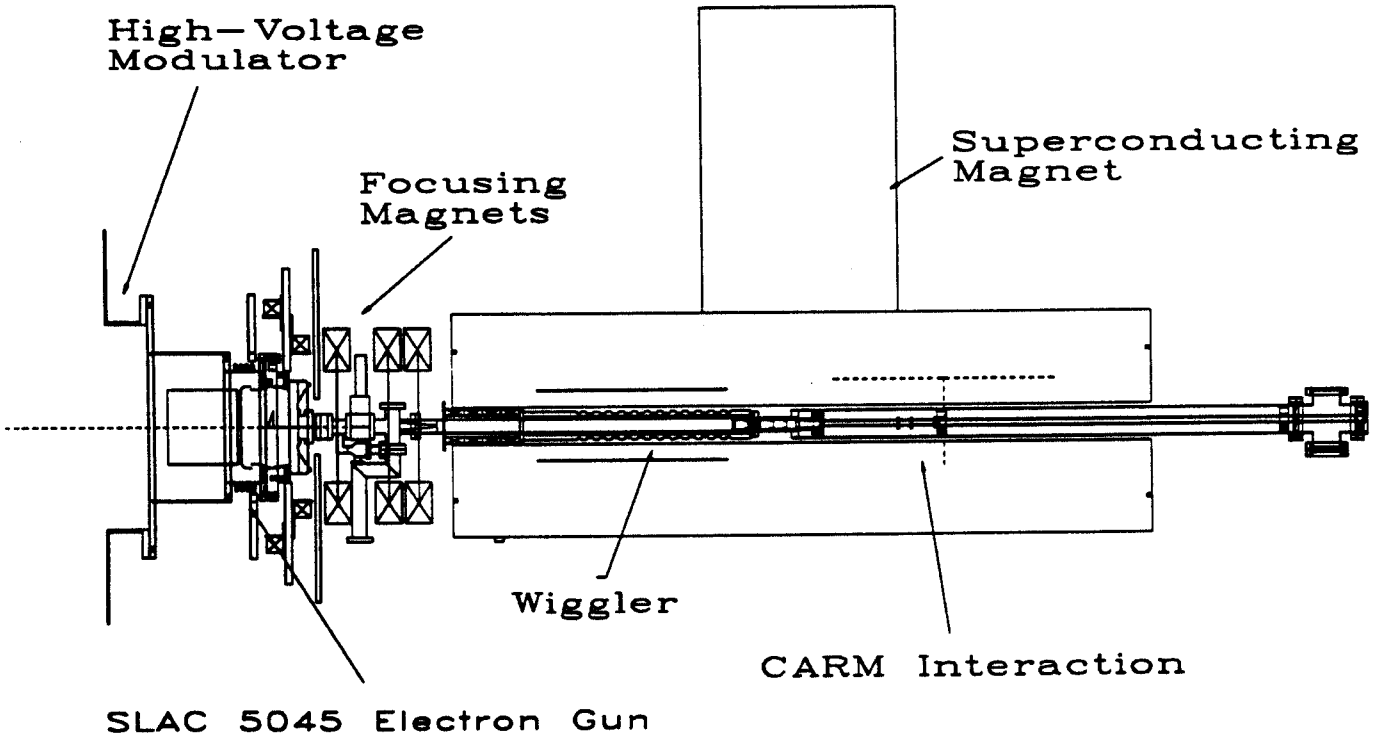

Figure 1: Schematic of the MIT long-pulse CARM oscillator experiment.

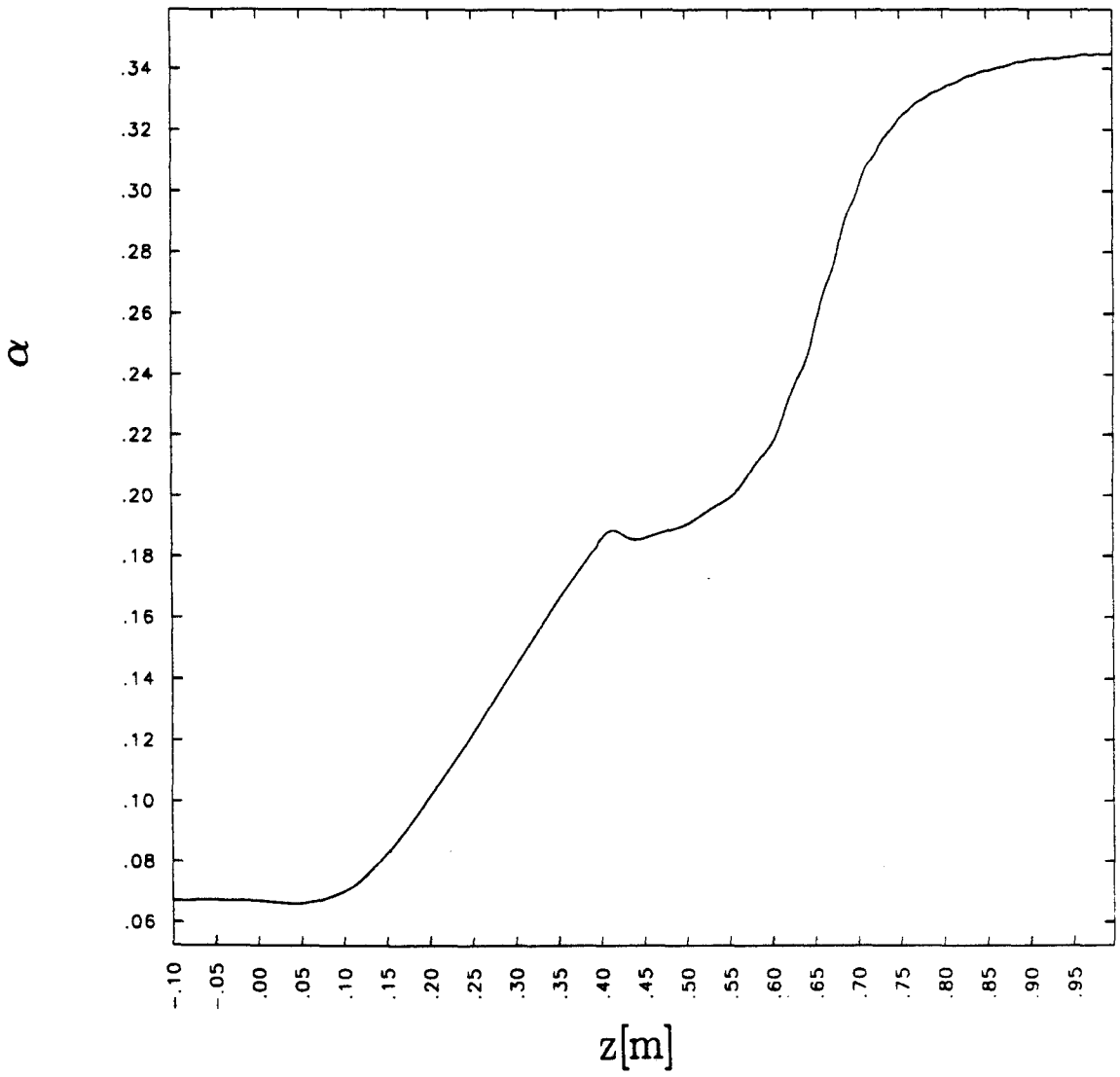

Figure 2: Average pitch angle (ordinate) as a function of axial distance z[m] as calculated from the wiggler electron trajectory code TRAJ. The helical windings start at z=0 and end at z=0.42 m. The adiabatic compression region begins at z≈0.45 m and ends at z≈1.0 m. Even with the self-fields, the compression into the interaction region from the wiggler region is nearly adiabatic. For this code run $\gamma = 1.552$, $I_w = 9.1A$, $B_{zw} = 1.84$ kG, and $B_{z0} = 6.36$ kG.

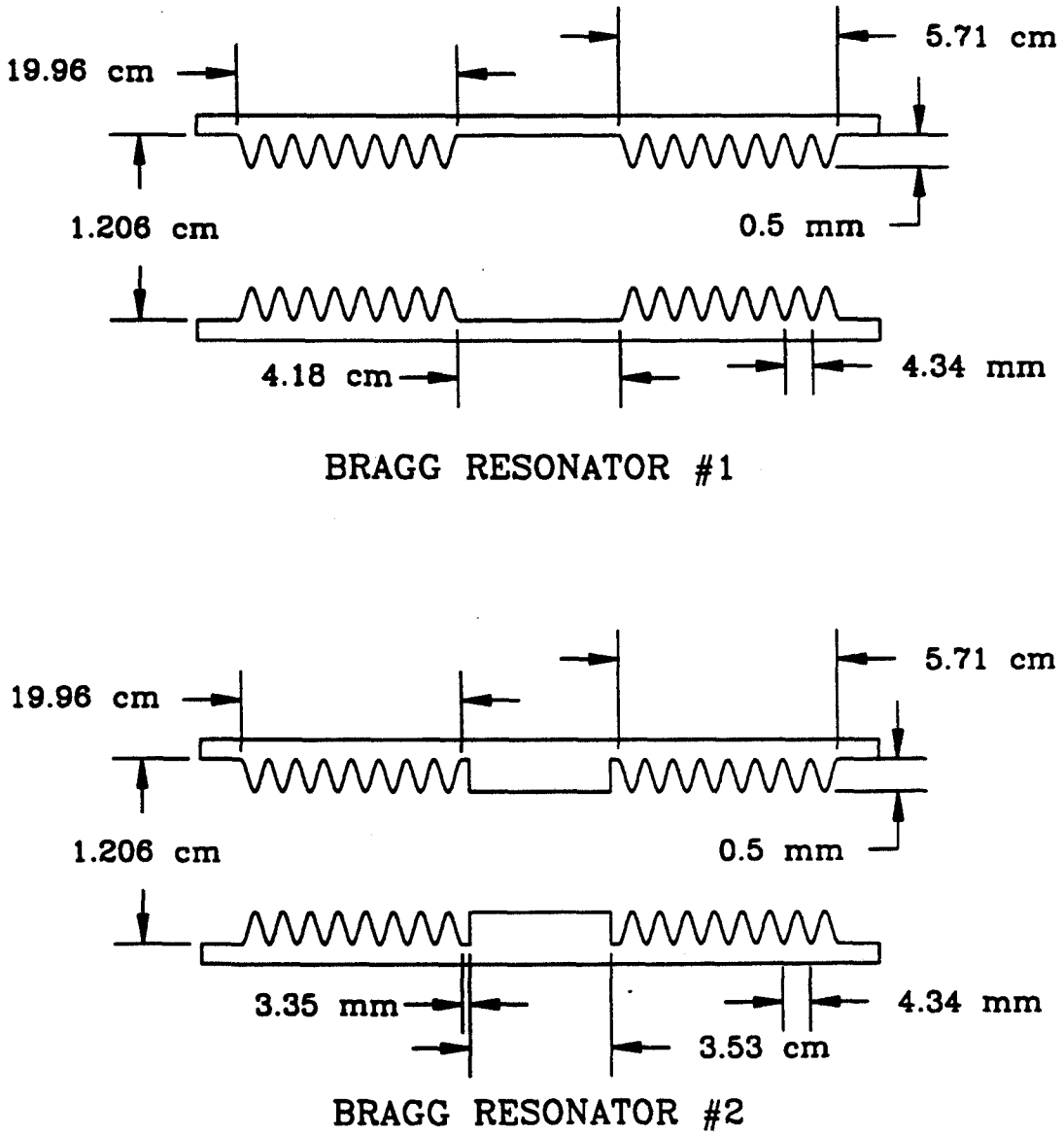

Figure 3: Schematic of the Bragg resonator cavities (not to scale). The electron beam enters through the long (upstream) reflector and exits from the short (downstream) reflector.

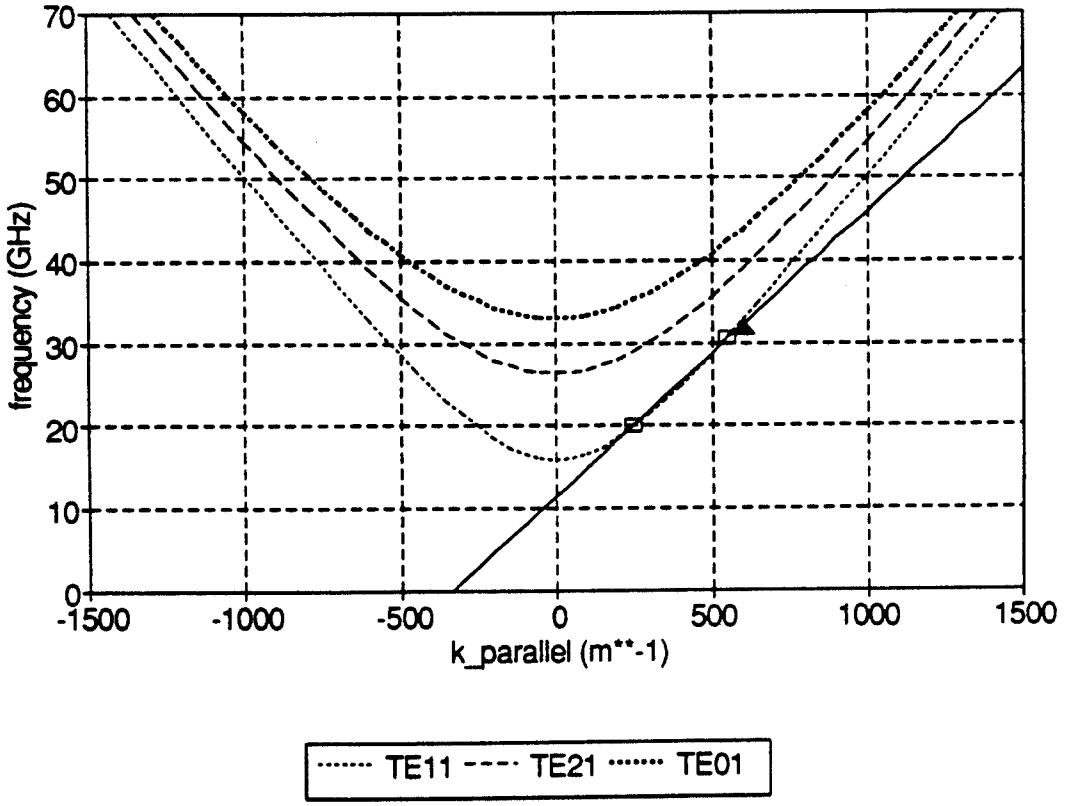

Figure 4: Theoretical intersections (squares) of the beamline with the TE_{11} waveguide mode observed for Cavity #2 and the measured frequency (triangle). $B_{z0} = 6.36$ kG, $\gamma = 1.552$, and $\alpha = 0.345$.

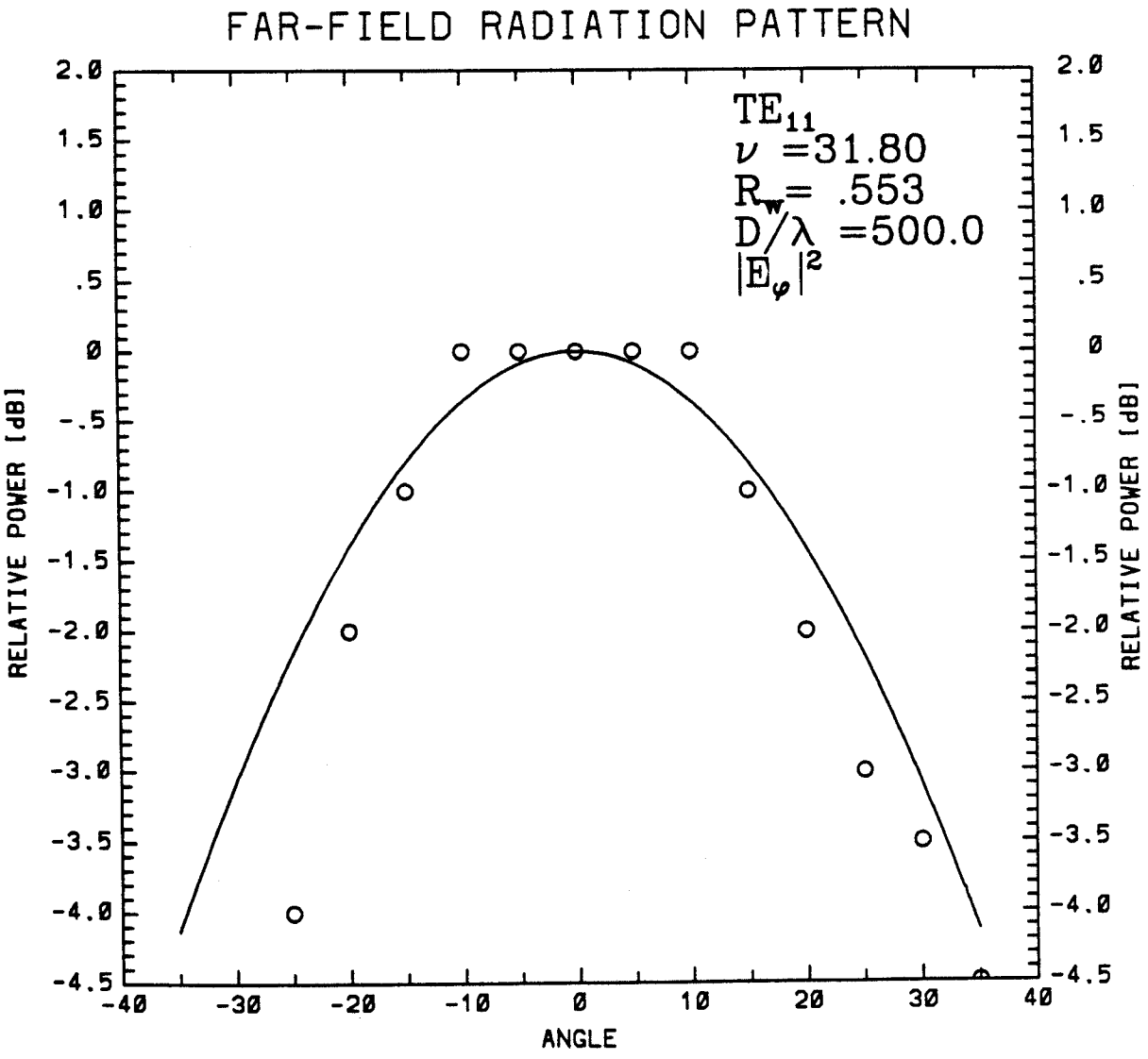

Figure 5: Measured relative power(circles) and theoretical farfield pattern(line) for the TE_{11} mode; ν in GHz, R_w in cm.

Resonator Parameters	Value
Long reflector length	19.95 cm
Power reflectivity, R_u	93 %
Short reflector length	5.71 cm
Power reflectivity, R_d	27 %
Straight section length	4.14 cm
Diffractive Q, Q_D	300
Ripple amplitude, δR	0.0254 cm
λ_b, Ripple period	4.34 cm
Cavity #1 radius	0.603 cm
Cavity #2 radius	0.553 cm
Mode	TE_{11}
Frequency	37.5 GHz

Table 1: CARM Bragg Resonator Design Parameters.

CARM Parameter	Value
Beam Voltage	260-320 kV
Beam Current	10-25 A
Pulse Length	$> 1\mu$sec
I_w, Wiggler Current	0-34 A
N_p, Wiggler Periods	6
r_h, Wiggler Radius	3.34 cm
N_w, Wiggler Windings	18
Frequency Range (Cavity #1)	24.8-40.1 GHz
Frequency Range (Cavity #2)	29.6-36.8 GHz

Table 2: MIT CARM Oscillator Experimental Parameters

Mode #	ν[GHz]	V[kV]	B_{zo}[kG]	α_i	P_{out}[kW]
30*	33.5	270	6.79	0.403	5.6
31*	30.2	300	7.44	0.477	0.07
32	30.3	300	7.44	0.381	N/A
33	29.7	300	6.21	0.454	0.2
34	30.9	300	6.21	0.459	0.7
35*	30.9	300	6.21	0.308	0.2
36	29.6	300	6.21	0.744	0.2
37*	31.0	300	6.21	0.249	2.0
38*	30.3	282	7.24	0.647	N/A
39*	31.6	282	6.69	0.217	0.4
40*	30.8	282	6.45	0.191	1.3
41*	31.8	282	6.36	0.345	3.1
42*	31.8	282	6.36	0.361	N/A
43	N/A	317	6.36	0.494	100
44	N/A	317	6.32	0.775	110

Table 3: Cavity #2 modes. Power is measured from a calibrated diode in the farfield radiation pattern. The (*) denotes a TE_{11} CARM mode identification from agreement with uncoupled mode dispersion theory. Other modes are unidentified.

References

[1]I.E. Botvinnik, V.L. Bratman, A.B. Volkov, G.G. Denisov, B.D. Kol'chugin, and M.M. Ofitserov, "The cyclotron autoresonance maser operated at a wavelength 2.4 mm",*Pis'ma Zh. Eksp. Teor. Fiz.*, Vol 8, pp. 1376-1378 (1982).

[2]A.W. Fliflet, R.B. McCowan, C.A. Sullivan, D.A. Kirkpatrick, S.H. Gold, and W.M. Manheimer, "Development of High Power CARM Oscillators", *Nuc. Inst. Meth. Phys. Res.*, Vol *A*285, pp. 233-238 (1989).

[3]K.D. Pendergast, B.G. Danly, R.J. Temkin, and J.S. Wurtele, "Self-Consistent Simulation of Cyclotron Autoresonance Maser Amplifiers," *IEEE Trans. Pl. Sci.*, Vol. 16, pp. 122–128 (1988).

[4]B.G. Danly, J.A. Davies, K.D. Pendergast, R.J. Temkin, and J.S. Wurtele,"High-Frequency Cyclotron Autoresonance Maser Amplifier Experiments at M.I.T.",*SPIE Microwave and Particle Beam Sources*, Vol. 1061, (1989).

[5]V.L. Bratman, N.S. Ginzburg, G.S. Nusinovich, M. I. Petelin, and P. S. Strelkov, "Relativistic Gyrotrons and Cyclotron Autoresonance Masers," *Int. J. Electron.*, Vol. 51, pp. 541–567 (1981).

[6]C. Chen and J.S. Wurtele, "Efficiency Enhancement in Cyclotron Autoresonance Maser Amplifiers by Magnetic Field Tapering", *Phys. Rev. A*, Vol 40, No. 1, pp. 489-491 (1989).

[7]A.W. Fliflet, "Linear and Nonlinear Theory of the Doppler–Shifted Cyclotron Resonance Maser Based on TE and TM Waveguide modes," *Int. J. Electron.*, Vol. 61, pp. 1049 –1080 (1986).

[8]A.T. Lin and C.C. Lin, "Doppler Shift Dominated Cyclotron Maser Amplifiers,"*Int. J. Infr. and Mill. Waves*, Vol. 6, pp. 41–51 (1985).

[9]G. Bekefi, A. DiRienzo, C. Leibovitch, and B.G. Danly, "35 GHz Cyclotron Autoresonance Maser Amplifier", *Appl Phys. Lett.*, Vol 54, No. 14, pp. 1302-1304 (1989).

[10]W. Mulligan, G. Bekefi, S.C. Chen, B.G. Danly, and R.J. Temkin, "A High-Voltage Modulator for High-Power RF Source Research", *1990 Nineteenth Power Modulator Symposium.*

[11]W.B. Herrmannsfeldt, "EGUN - An Electron Optics and Gun Design Program", Stanford Linear Accelerator Center.

[12]Los Alamos Accelerator Code Group, "Poisson/Superfish Group of Codes", Los Alamos National Laboratory, MS H829.

[13]R.H. Jackson and C.A. Sedlak, "Gyrotron Beam Generation With Helical Magnetic Fields", Final report for NRL, MRC/WDC-R-061, (1983).

[14]V.L. Bratman, G.G. Denisov, N.S. Ginzburg, and M. I. Petelin, "FEL's with Bragg Reflection Resonators: Cyclotron Autoresonance Masers Versus Ubitrons," *IEEE J. Quant. Elec.*, Vol. $\underline{QE-19}$, pp. 282–296 (1983).

[15]R.B. McCowan, A.W. Fliflet, S.H. Gold, V.L. Granatstein, and M.C. Wang, "Design of a Waveguide Resonator With Rippled Wall Reflectors for a 100 GHz CARM Oscillator Experiment", *Int. J. Electronics*, Vol 65, No. 3, pp. 463-475 (1988).

[16]G.G. Denisov and M.G. Reznikov, "Corruated Cylindrical Resonators for Short-Wavelength Relativistic Microwave Oscillators", *Iz. Vyss. Uch. Zav. Rad.*, Vol 25, No. 5, pp. 407-413 (1982).